Dalton Transactions

Accepted Manuscript

ROYAL SOCIETY OF CHEMISTRY

www.rsc.org/dalton

Graphic Abstract

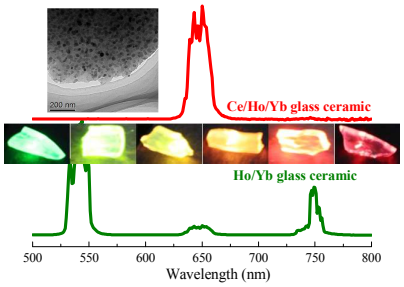

First report of single-band red upconversion in Yb^{3+}/Ho^{3+} activated nano-glass-ceramics through Ce^{3+} doping

Tuning into single-band red upconversion luminescence in Yb^{3+}/Ho^{3+} activated nano-glass-ceramics through Ce^{3+} doping

Daqin Chen [a,b,*], Yang Zhou [a], Zhongyi Wan [a], Zhenguo Ji [a], Ping Huang [b,*]

[a] College of Materials & Environmental Engineering, Hangzhou Dianzi University, Hangzhou, 310018, P. R. China

[b] State Key Laboratory of Structural Chemistry, Fujian Institute of Research on the Structure of Matter, Chinese Academy of Sciences, Fuzhou, Fujian 350002, PR China

Abstract: Yb^{3+}/Ho^{3+} activated glass ceramics containing β-YF_3 nanocrystals was successfully fabricated. The green ($^5S_2/^5F_4 \rightarrow ^5I_8$) upconversion emission is dominant in the glass ceramic and is about 160 times stronger than that of the precursor glass, which is resulted from the partition of lanthanide activators into low-phonon-energy crystalline lattice and subsequently the low probability of multi-phonon nonradiative relaxation from the $^5S_2/^5F_4$ and $^5I_6$ states to the lower ones. Upon introduction of Ce^{3+} ions into nano-glass-ceramics, two efficient cross-relaxation processes between Ho^{3+} and Ce^{3+}, i.e, Ho^{3+}: $^5S_2/^5F_4$ + Ce^{3+}: $^2F_{5/2}$ → Ho^{3+}: $^5F_5$ + Ce^{3+}: $^2F_{7/2}$ and Ho^{3+}: $^5I_6$ + Ce^{3+}: $^2F_{5/2}$ → Ho^{3+}: $^5I_7$ + Ce^{3+}: $^2F_{7/2}$, are demonstrated to greatly suppress the population of green-emitting $^5S_2/^5F_4$ state and enhance the population of red-emitting $^5F_5$ one, leading to intense single-band red UC radiation of Ho^{3+}.

Corresponding authors:
E-Mail: dqchen@hdu.edu.cn (D. Q. Chen)
phuang@fjirsm.ac.cn (P. Huang)

Photon upconversion (UC) is a nonlinear photophysical process characterized by the conversion of long-wavelength radiation into short-wavelength one [1-5]. The large anti-Stokes shift between excitation and emission is based on the sequential absorption of two or more low-energy photons by metastable, long-living energy states followed by the emission of one higher-energy photon. It is well-known that lanthanide (Ln^{3+}) activators doped in the appropriate hosts generally have abundant meta-stable excited states, which enable them to emit photons covering from ultraviolet to infrared spectral region. Unfortunately, this kind of multiple-band emission characteristics induces energy de-concentration, and is disadvantage to achieving high-efficient UC emission for a specific Ln^{3+} emitting state. Therefore, searching special UC hosts [6-8] and/or energy transfer routes [9-12] to achieve single-band and high-efficient emission of Ln^{3+} remains a formidable challenge, but is highly desirable.

Herein, using nano-glass-ceramics as UC host, we demonstrated the realization single-band red UC luminescence in Yb^{3+}/Ho^{3+} couple via energy transfer with the help of Ce^{3+} doping. Such nanostructured composite is achieved by controlled crystallization of the precursor glass with appropriate chemical composition, and the key factor for the efficient single-band red UC luminescence is the partition of the optically active Ln^{3+} ions into the precipitated nanocrystals (NCs). In this case, such nanocomposite may combine the favorable properties from both crystals and glasses, i.e., special crystal field environments for optically active dopants and high mechanical, chemical stabilities as well as easy-fabrication [13-21].

The materials were prepared with the following composition (in mol%): (42.9-x) SiO_2-28Al_2O_3-17NaF-11YF_3-1YbF_3-0.1HoF_3-xCeF_3 (x =0, 0.1, 0.25, 0.5, 1.0 and 2.0). The chemicals were mixed thoroughly and melted in a covered Pt crucible at 1450 ℃ for 30 min in the ambient atmosphere. The melt was poured into a copper mold and cooled down naturally to room temperature to form the precursor glass (PG), which was then heat-treated to 670 ℃ and hold for 2 h to form glass ceramic (denoted as GC0, GC1, GC2, GC3, GC4 and GC5 for x=0, 0.1, 0.25, 0.5, 1.0 and 2.0 respectively) through fluoride crystallization.

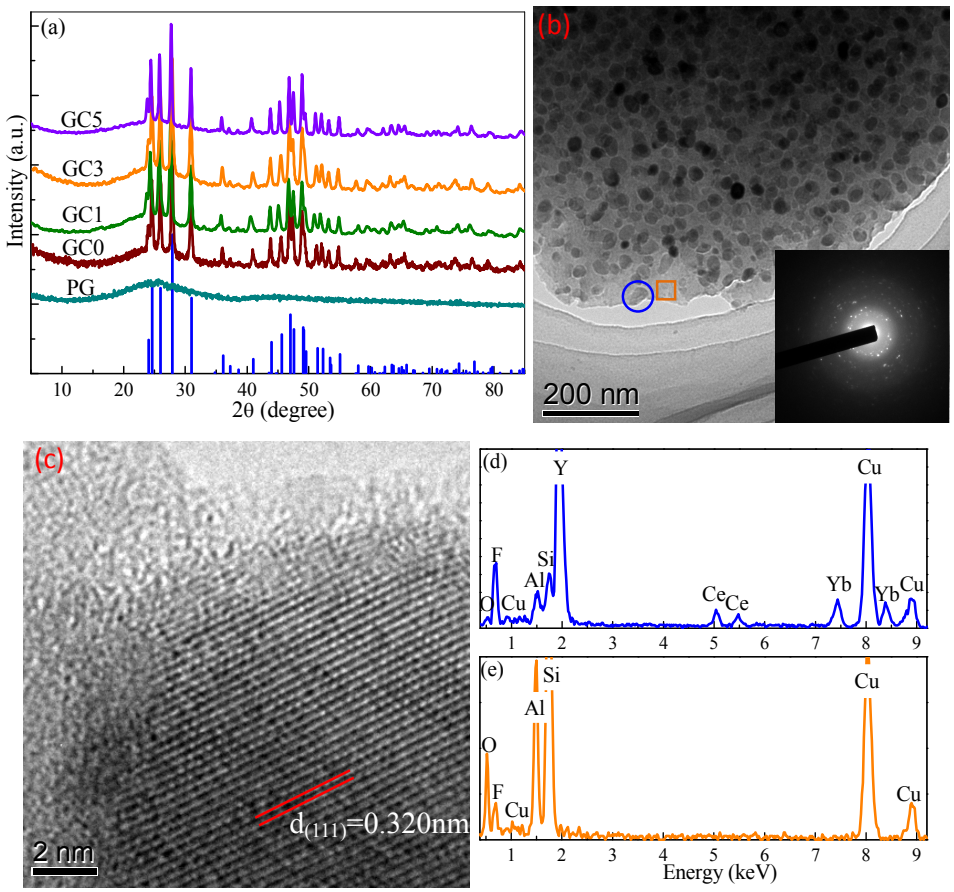

Figure 1 (a) XRD patterns of PG, GC0, GC1, GC3 and GC5 samples; bars represent the diffraction pattern of the standard orthorhombic β-YF_3 (JCPDS no. 74-0911) phase. (b) TEM image of GC3 and (c) HRTEM micrograph of an individual NC; inset of (b) shows SAED pattern of the corresponding sample. EDX spectra taken from (d) an individual YF_3 nanoparticle and (e) the glass matrix in GC3.

X-ray diffraction (XRD) patterns of the PG and GCs are given in Figure 1a. PG does not exhibit any discrete diffraction peaks, confirming its amorphous nature. After crystallization, intense diffraction peaks assigned to the orthorhombic β-YF_3 crystals (JCPDS No. 74-0911) appear in all the GC samples, indicative the precipitation of pure YF_3 among glass matrix. Transmission electron microscopy (TEM) image of the GC3 sample (Figure 1b) demonstrates that nanoparticles sized 15-25 nm are dispersed homogeneously among the glass matrix with their selected area electron diffraction (SAED) rings well indexed to the orthorhombic β-YF_3. High-resolution TEM (HRTEM) image (Figure 1c) confirms the high crystallinity of YF_3 phase. To detect the distribution of Ln^{3+} ions in GC, energy dispersive x-ray (EDX) spectra with nano-sized

probe taken from an individual YF_3 NC and the glass matrix were recorded. As revealed in Figure 1d, the spectrum of an individual nanoparticle shows Y, F, Ce and Yb peaks (Cu signals come from the copper grid, Ho signal is not detected owing to the low doping content). Other weak Al, Si, and O signals are originated from the glass matrix surrounding the crystalline phase. However, no Ln^{3+} signal is observed in the EDX spectrum of the glass matrix (Figure 1e). These results indicate that the lanthanide dopants (Ce^{3+}, Yb^{3+} and Ho^{3+}) mainly segregate in the precipitated YF_3 crystalline phase after glass crystallization.

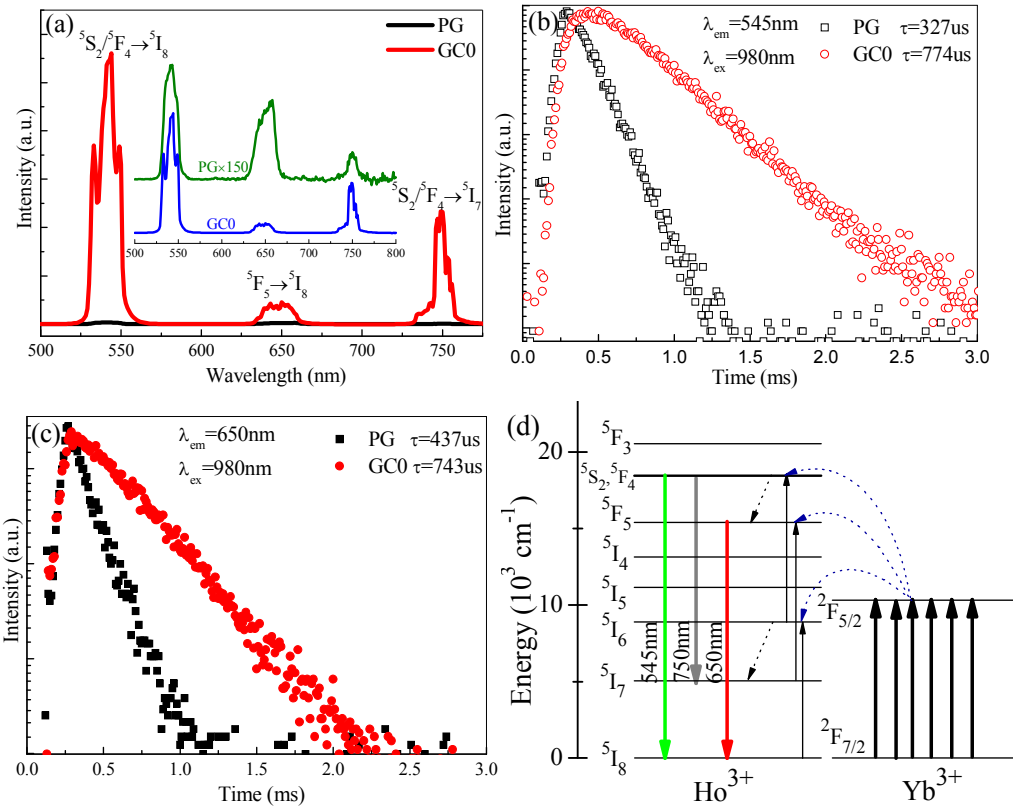

Figure 2 (a) UC emission spectra of PG and GC0 samples without the addition of Ce^{3+} ions. UC decay curves corresponding to (b) Ho^{3+} $^5S_2/^5F_4$ and (c) $^5F_5$ states in PG and GC0. (d) Energy level diagrams of Ho^{3+} and Yb^{3+} as well as the proposed green and red UC mechanisms in PG and GC0.

The influence of the glass crystallization on the UC optical performance of the Yb^{3+}/Ho^{3+} activated GC0 samples is investigated, as shown in Figure 2a. Under 980 nm NIR laser excitation, both the PG (without Ce^{3+} doping) and GC0 samples exhibit emission bands located at 545 (green), 650 (red), and 750 nm (NIR) corresponding to

$^5S_2/^5F_4 \rightarrow {}^5I_8$, $^5F_5 \rightarrow {}^5I_8$, and $^5S_2/^5F_4 \rightarrow {}^5I_7$ transitions of Ho^{3+}, respectively. Impressively, the UC intensity of Ho^{3+} in GC0 is far stronger than that in PG, i.e., the green, red and NIR UC luminescence enhances by 160, 18 and 200 times, respectively, indicating the alteration of the crystal field for Ho^{3+} ions after ceramization. Fluorescence lifetimes of Ho^{3+} UC emissions can further discover the surroundings where Ho^{3+} stayed. Figure 2b-2c show UC decay curves for Ho^{3+}: $^5S_2/^5F_4$ and $^5F_5$ states in PG and GC0 under 980 nm laser excitation. Compared with those in PG, the lifetimes of Ho^{3+} in GC apparently increase. Longer lifetimes of UC emissions confirm the low nonradiative de-excitation of Ho^{3+} ions in GC0, i.e., Ho^{3+} ions are incorporated into YF_3 crystalline lattice with low-phonon-energy. The partition of Ln^{3+} ions in the precipitated fluoride nanophase has also been observed in other GCs [13-21].

The dependence of green or red emission intensity on the pump power is nearly quadratic (not shown here) for both PG and GC0 samples, indicating that two-photon UC process is responsible for the population of the Ho^{3+} $^5S_2/^5F_4$ and $^5F_5$ states. Figure 2d exhibits the proposed UC mechanisms for the investigated PG and GC0. Once the sensitizers (Yb^{3+} ions) are populated through ground state absorption (GSA) under NIR laser excitation, the successive two-step energy transfers (ETs) from Yb^{3+} to Ho^{3+} will populate $^5I_6$ and then $^5S_2/^5F_4$ states of Ho^{3+}, where green ($^5S_2/^5F_4 \rightarrow {}^5I_8$) and NIR ($^5S_2/^5F_4 \rightarrow {}^5I_7$) emissions yield. With the help of non-radiative relaxation from $^5S_2/^5F_4$ states to $^5F_5$ one, red ($^5F_5 \rightarrow {}^5I_8$) emission produces. In addition, the population of $^5F_5$ state can also be achieved through another ET process of Yb^{3+}: $^2F_{5/2}$ + Ho^{3+}: $^5I_7 \rightarrow Yb^{3+}$: $^2F_{7/2}$ + Ho^{3+}: $^5F_5$, where the Ho^{3+}: $^5I_7$ state is populated from Ho^{3+}: $^5I_6$ one through non-radiative deactivation. Apparently, the improvement in UC performance in GC0 is ascribed to the surroundings alteration of Ho^{3+} ions after crystallization. The maximum phonon energy of the aluminosilicate glass is about 1100 cm^{-1} [22], while that of YF_3 is around 400 cm^{-1} [23-24]. For the precursor glass, the high probability of multi-phonon nonradiative relaxation of Ho^{3+} leads to the weak UC luminescence and the high red to green emission ratio. However, for the glass ceramic, the population of Ho^{3+} ions at $^5I_6$ and $^5S_2/^5F_4$ levels is high since Ho^{3+} ions are preferentially incorporated into low-phonon-energy YF_3 lattice and subsequently have low

multi-phonon nonradiative relaxation, leading to the intense UC luminescence as well as the low red to green ratio.

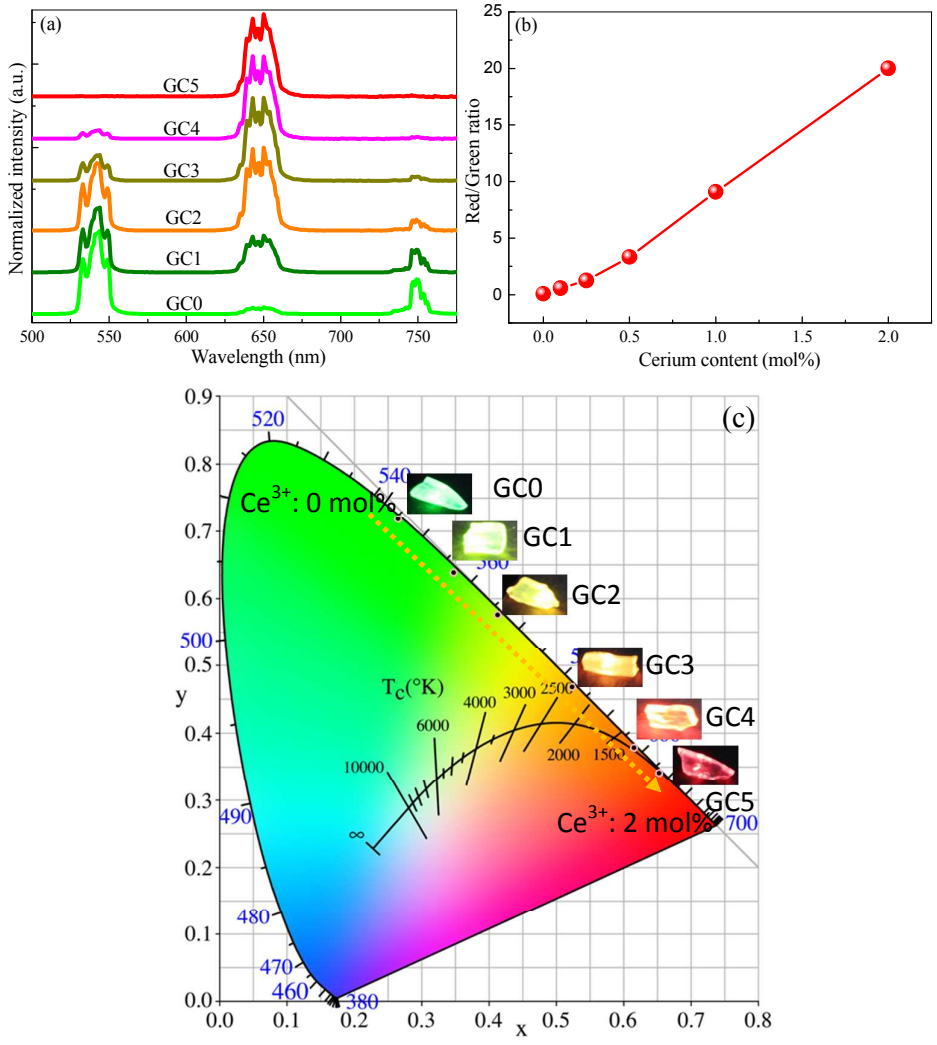

Figure 3 (a) Normalized UC emission spectra of Yb^{3+}/Ho^{3+} activated GCs doped with different content of Ce^{3+} ions; (b) the dependence of UC red to green ratio on Ce^{3+} content; (c) CIE coordinate diagram showing chromaticity points of GCs; Insets of (c) are the UC luminescent photographs of the corresponding GC samples.

Figure 3a presents the impact of Ce^{3+} doping on UC luminescence of Yb^{3+}/Ho^{3+} activated nano-glass-ceramics (GC0, GC1, GC2, GC3, GC4, GC5). To clearly clarify the color tunablity, all the UC spectra have been normalized to the maximum value of emission band. Impressively, the UC intensity ratios of red to green as well red to NIR are greatly enhanced with increase of Ce^{3+} content, and nearly single-band red UC

emission is realized when Ce^{3+} content reaches 2 mol%. These results demonstrate the significance of Ce^{3+} dopants for the UC tuning from green to red in GC, as evidenced by the gradual enhancement of the intensity ratio of red to green with increase of Ce^{3+} content (Figure 3b). To visualize the UC color modification induced by Ce^{3+} doping, photographs of the UC luminescence for GC0, GC1, GC2, GC3, GC4 and GC5 samples, under 980 nm laser excitation, are provided in the inset of Figure 3c. Obviously, the UC colors can be finely tuned from pure green to yellow and finally to pure red, as evidenced by the variation of chromaticity coordinates in the Commission International de l'Eclairage (CIE) 1931 chromaticity diagram (Figure 3c), and the changes in the UC color with increasing Ce^{3+} doping content are clearly visible by the naked eyes.

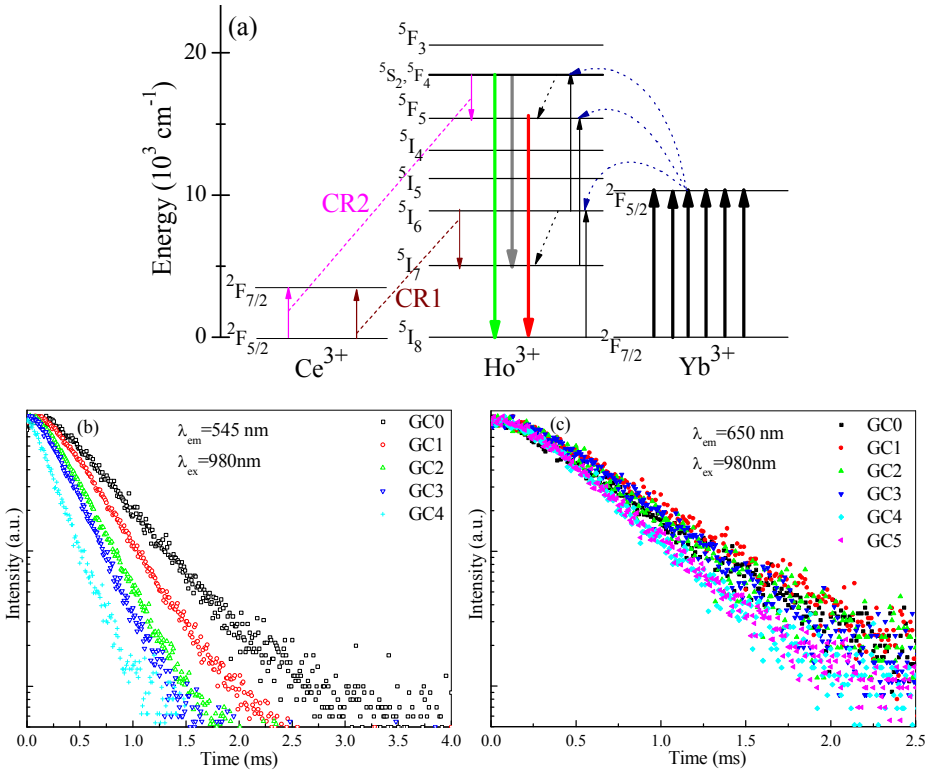

Figure 4 (a) Energy level diagrams of Ce^{3+}, Ho^{3+} and Yb^{3+} as well as the proposed mechanisms for the realization of single-band red UC luminescence. UC decay curves corresponding to (b) Ho^{3+} $^5S_2/^5F_4$ and (c) $^5F_5$ states in GCs as a function of Ce^{3+} doping content.

Table 1 Lifetime values for Ho^{3+} $^5S_2/^5F_4$, $^5I_6$ and $^5F_5$ states in GCs

sample	$^5S_2/^5F_4$ (μs)	$^5I_6$ (μs)	$^5F_5$ (μs)
GC0	774	192	655
GC1	572	156	762
GC2	443	121	727
GC3	387	97	695
GC4	234	74	589
GC5	---	52	578

Figure 4a shows energy levels of Ce^{3+}, Ho^{3+} and Yb^{3+} ions as well as the proposed mechanisms to explain the realization of single-band red UC emission in GCs. The Ho^{3+}: $^5S_2/^5F_4$ green-emitting states are populated by the same UC processes as above-mentioned since there are not matching energy gaps from Ho^{3+}: $^5S_2/^5F_4$ state to the lower/higher one as the energy gap of Ce^{3+} ion between $^2F_{7/2}$ and $^2F_{5/2}$ (~3000 cm^{-1}) [25-26]. As evidenced by EDX analyses (Figure 1d-1e) and UC emission results (Figure 2), the Ln^{3+} dopants (including Ce, Yb and Ho) incorporated in the YF_3 NCs after glass crystallization. The maximum phonon energy of YF_3 crystal is about 400 cm^{-1} [23]. Therefore, six and eight phonons are required to bridge the energy gaps for the $^5S_2$ to $^5F_5$ (2450 cm^{-1}) and between $^5I_6$ and $^5I_7$ (3450 cm^{-1}), respectively, and subsequently the nonradiative relaxation probability from $^5S_2$ or $^5I_6$ states to the lower ones is quite low, which results in the low red to green UC emission ratio in GC0 sample (without Ce^{3+} doping), as evidenced in Figure 2a. However, for GC1-GC5 samples with increase of Ce^{3+} content, the red to green ratio monotonously increases (Figure 3a-3b), confirming that Ce^{3+} dopants play the key role in enhancing Ho^{3+} red UC emission and weakening green one. Herein, two cross-relaxation processes involving Ce^{3+} and Ho^{3+} (i.e., CR1: Ho^{3+}: $^5I_6$ + Ce^{3+}: $^2F_{5/2}$→Ho^{3+}: $^5I_7$ + Ce^{3+}: $^2F_{7/2}$ and CR2: Ho^{3+}: $^5S_2/^5F_4$ + Ce^{3+}: $^2F_{5/2}$→Ho^{3+}: $^5F_5$ + Ce^{3+}: $^2F_{7/2}$) were proposed to explain the observed phenomena because the energy gaps of Ho^{3+}: $^5I_6$-$^5I_7$ as well as Ho^{3+}: $^5S_2/^5F_4$-$^5F_5$ are approximatively matched with that of Ce^{3+}: $^2F_{7/2}$-$^2F_{5/2}$. These two CR processes are beneficial to depopulating the electrons in the green-emitting $^5S_2/^5F_4$

state and its intermediate $^5I_6$ one, while populating the red-emitting $^5F_5$ state and its intermediate state $^5I_7$ one. Since the segregation of Ln^{3+} in YF_3 lattice results in the short ionic-ionic distances and subsequently the strong interaction between Ho^{3+} and Ce^{3+} ions, these two CR processes will occur efficiently with increase of Ce^{3+} content. As a consequence, single-band red UC radiation is easily realized through greatly weakening green and NIR UC emissions when Ce^{3+} content is high enough (2 mol% in the present GC system). To prove the existence of the CR processes, UC decay profiles corresponding to Ho^{3+} $^5S_2/^5F_4$, $^5I_6$ and $^5F_5$ states in GCs as a function of Ce^{3+} doping content were measured, as shown in Figure 4b-4c and tabulated in Table 1. Because of the non-exponential nature of the decay curves for the GC samples, the experimental lifetime was calculated by $\tau_{\exp} = \int I(t)dt / I_p$, where *I(t)* represents the function of the luminescence intensity on the time *t*, and I_p the peak intensity in the decay curve. With increase of Ce^{3+} doping content, the gradual decrease for the lifetimes of the green-emitting Ho^{3+} $^5S_2/^5F_4$ state and the intermediate state $^5I_6$ clearly evidences the occurrence of CR2 and CR1. Importantly, the lifetime for the red-emitting $^5F_5$ state is not greatly affected by Ce^{3+} doping, which ensures intense red UC emission in the present nano-glass-ceramics.

As a comparison, we have also carried out experimental investigation on the Yb/Ho/Ce tri-doped YF_3 NCs and observed the similar results, as shown in Figure S1 (Electronic Supplementary Information). XRD analysis and TEM observation confirm the successful synthesis of pure YF_3 NCs. Evidently, green UC emission is dominant in the Yb/Ho co-doped product. With the introducing of Ce^{3+} dopants into Yb/Ho: YF_3 NCs, nearly single-band red UC luminescence is observed, which is similar to the case of the Yb/Ho/Ce: YF_3 NCs embedded GC. Most recently, the same CR mechanisms have also been demonstrated in the Yb/Ho/Ce: $NaY_{0.6}Gd_{0.4}F_4$ nanocrystals [12].

It is worthy to be mentioned that the investigated GC with single-band red UC luminescence might find potential application in enhancing sunlight harvesting for photosynthesis of agricultural plants. Generally, the green plants (chlorophylls) absorb more reddish orange (600-700 nm) lights than other wavelengths during

photosynthesis [27-28]. In the solar spectrum, the energy percentages of the ultraviolet, visible, and infrared light are 7%, 50%, and 43%, respectively [29]. The lights absorbed by green plants for photosynthesis are only a very small part in the whole solar spectrum. Therefore, the present nano-glass-ceramics may act as the light-converted window to improve the utilization of solar and increase production of green plants after further optimizing glass-ceramic structure and optical performance.

In summary, UC luminescence tuning from green to red in the Yb^{3+}/Ho^{3+} activated GCs containing β-YF_3 NCs was successfully realized via Ce^{3+} doping under 980 nm laser excitation. Without the addition of Ce^{3+} dopants, the green ($^5S_2/^5F_4 \rightarrow ^5I_8$), red ($^5F_5 \rightarrow ^5I_8$) and NIR ($^5S_2/^5F_4 \rightarrow ^5I_7$) emissions of Ho^{3+} in the glass ceramic are about 160, 18 and 200 times stronger than those in the precursor glass due to the incorporation of Ln^{3+} activators into low-phonon-energy YF_3 crystalline lattice. Impressively, introducing Ce^{3+} into GC greatly enhances the UC intensity ratios of red to green as well red to NIR, and results in intense single-band red UC emission. Two efficient CR processes, i.e., Ho^{3+}: $^5S_2/^5F_4$ + Ce^{3+}: $^2F_{5/2}$ → Ho^{3+}: $^5F_5$ + Ce^{3+}: $^2F_{7/2}$ and Ho^{3+}: $^5I_6$ + Ce^{3+}: $^2F_{5/2}$ → Ho^{3+}: $^5I_7$ + Ce^{3+}: $^2F_{7/2}$, are confirmed to be responsible for this UC color tunability.

Acknowledgements

This work was supported by the National Natural Science Foundation of China (21271170, 61372025 and 51402077).

Electronic Supplementary Information (ESI) available: Experimental details of synthesizing the Yb/Ho/Ce: YF_3 nanocrystals and Figure **S1**.

References

[1] E. Downing, L. Hesselink, J. Ralston and R. Macfarlane, *Science*, 1996, **273**, 1185.

[2] F. Auzel, *Chem. Rev.*, 2004, **104**, 139.

[3] F. Wang, Y. Han, C. Lim, Y. Lu, J. Wang, J. Xu, H. Chen, C. Zhang, M. Hong and X.G. Liu, *Nature*, 2010, **463**, 1061.

[4] D.Q. Chen, Y.S. Wang and M.C. Hong, *Nano Energy*, 2012, **1**, 73.

[5] S. Gai, C. Li, P. Yang and J. Lin, *Chem. Rev.*, 2014, **114**, 2343.

[6] D. Q. Chen, L. Lei, R. Zhang, A. P. Yang, J. Xu and Y. S. Wang, *Chem. Commun.*, 2012, **48**, 10630.

[7] G. Yi, Y. Peng and Z. Gao, *Chem. Mater.*, 2011, **23**, 2729.

[8] J. Wang, R. Deng, M. A. MacDonald, B. Chen, J. Yuan, F. Wang, D. Chi, T. S. Andy Hor, P. Zhang, G. Liu, Y. Han and X. Liu, *Nat. Mater.*, 2014, **13**, 157.

[9] J. Wang, F. Wang, C. Wang, Z. Liu and X. G. Liu, *Angew. Chem. Int. Ed.*, 2011, **50**, 10369.

[10] G. Tian, Z. J. Gu, L. J. Zhou, W. Y. Yin, X. X. Liu, L. Yan, S. Jin, W. L. Ren, G. M. Xing, S. Y. Li and Y. L. Zhao, ***Adv. Mater.***, 2012, **24**, 1226.

[11] G. Chen, H. Liu, G. Somesfalean, H. Liang and Z. Zhang, *Nanotechnology*, 2009, **20**, 385704.

[12] W. Gao, H. Zheng, Q. Han, E. He, F. Gao and R. Wang, *J. Mater. Chem. C*, 2014, **2**, 5327.

[13] D. Q. Chen, Z. Wan, Y. Zhou, Y. Chen, H. Yu, H. W. Lu, Z. G. Ji and P. Huang, *J. Alloys Compd.*, 2015, **625**, 149.

[14] D. Q. Chen, W. Xiang, X. Liang, J. Zhong, H. Yua, M. Ding, H. Lu and Z. Ji, *J. Euro. Ceram. Soc.*, 2015, **35**, 859.

[15] S.L. Zhao, X.L. Wang, X. Sun, G.H. Jia, L.H. Huang, D.G. Deng, F.X. Xin and S.Q. Xu, *CrystEngComm*, 2013, **15**, 7346.

[16] Y.L. Wei, H.M. Yang, X.M. Li, L.J. Wang and H. Guo, *J. Am. Ceram. Soc.*, 2014, **97**, 2012.

[17] G. Wu, S. Fan, Y. Zhang, C. Chai, Z. Ma, M. Peng, J. Qiu and G. Dong, *Opt. Lett.*, 2013, **38**, 3071.

[18] X. P. Fan, X. S. Qiao, D. Zhao, Q. Luo and X. H. Zhang, *J. Alloys Compd.*, 2012, **511**, 232.

[19] A. Herrmann, M. Tylkowski, C. Bocker and C. Rüssel, *Chem. Mater.*, 2013, **25**, 2878.

[20] A.C. Yanes, A. Santana-Alonso, J. Méndez-Ramons, J. del-Castillo, V.D. Rodríguez, *Adv. Funct. Mater.*, 2011, **21**, 3136.

[21] S. F. Zhou, Q. Guo, H. Inoue, Q. Ye, A. Masuno, B. Zheng, Y. Yu and J. R. Qiu, *Adv. Mater.*, 2014, **26**, 7966.

[22] D. Zhao, X. Qiao, X. Fan and M. Wang, *Physica B*, 2007, **395**, 10.

[23] M. M. Lage, A. Righi, F. M. Matinaga, J. Y. Gesland and R. L. Moreira, *J. Phys.: Condens. Matter*, 2004, **16**, 3207.

[24] D. Q. Chen, Y. L. Yu, P. Huang, F. Weng, H. Lin and Y. Wang, *CrystEngComm*, 2009, **11**, 1686.

[25] N. C. Chang, J. B. Gruber, R. P. Leavitt and C. A. Morrison, *J. Chem. Phys.*, 1982, **76**, 3877.

[26] R. P. Leavitt, J. B. Gruber, N. C. Chang and C. A. Morrison, *J. Chem. Phys.*, 1982, **76**, 4775.

[27] C. Ming, F. Song, X. Ren and L. An, *Appl. Phys. Lett.*, 2013, **103**, 041906.

[28] C. Ming, F. Song, L. An and X. Ren, *Appl. Phys. Lett.*, 2013, **102**, 141903.

[29] D. Q. Chen, Y. S. Wang and M. C. Hong, *Nano Energy*, 2012, **1**, 73.